Anomalous metallic state and anisotropic multiband superconductivity in $Nb_3Pd_{0.7}Se_7$

Q. R. Zhang,[1] D. Rhodes,[1] B. Zeng,[1] T. Besara,[1] T. Siegrist,[1,2] M. D. Johannes,[3] and L. Balicas[1,*]

[1]*National High Magnetic Field Laboratory, Florida State University, Tallahassee, Florida 32310, USA*

[2]*Department of Chemical and Biomedical Engineering, Florida State University, Tallahassee, Florida 32310, USA*

[3]*Center for Computational Materials Science, Naval Research Laboratory, Washington, DC 20375, USA*

We report the discovery of superconductivity in $Nb_3Pd_xSe_7$ with an x-dependent superconducting transition temperature as high as $T_c \simeq 2.1$ K for $x \simeq 0.7$ (middle point of the resistive transition). Needlelike single crystals display anisotropic upper-critical fields with an anisotropy $\gamma = H_{c2}^b/H_{c2}^a$ as large as 6 between fields applied along their needle axis (or b axis) or along the a axis. As for the Fe based superconductors γ is temperature-dependent, suggesting that $Nb_3Pd_{0.7}Se_7$ is a multiband superconductor. This is supported by band structure calculations which reveal a Fermi surface composed of quasi-one-dimensional and quasi-two-dimensional sheets of hole character, as well as three-dimensional sheets of both hole and electron character. Remarkably, H_{c2}^b is observed to saturate at $H_{c2}^b(T \rightarrow 0$ K$) \simeq 14.1$ T which is $4.26 \times H_p$ where H_p is the Pauli-limiting field in the weak-coupling regime. The synthesis procedure yields additional crystals belonging to the $Nb_2Pd_xSe_5$ phase which also becomes superconducting when the fraction of Pd is varied. For both phases we find that superconductivity condenses out of an anomalous metallic state, i.e., displaying $\partial\rho/\partial T < 0$ above T_c similarly to what is observed in the pseudogap phase of the underdoped cuprates. An anomalous metallic state, low-dimensionality, multiband character, extremely high and anisotropic H_{c2}'s are all ingredients for unconventional superconductivity.

I. INTRODUCTION

The Fe chalcogenide compounds, such as $Fe_{1+\delta}Se$, $Fe_{1+\delta}Se_xTe_{1-x}$, or the $A_xFe_{2-y}Se_2$ ($A =$ Tl, Rb, or K) display remarkable superconducting properties. For example, the tetragonal phase of $Fe_{1+\delta}Se$ (i.e., when $0.01 \leqslant \delta \leqslant 0.04$) displays superconductivity at $T_c \sim 8.5$ K only when $\delta = 0.01$,[1] although it was recently shown that intercalation with $Li_x(NH_2)_y(NH_3)_{1-y}$ or K leads to a dramatic enhancement in T_c up to 43 K[2] and 44 K,[3] respectively. For the $Fe_{1+\delta}Se_xTe_{1-x}$ series, recent angle resolved photoemission studies suggest a ratio for the superconducting gap to the Fermi energy $\Delta/\varepsilon_F \approx 0.5$, placing this system at the BCS to BEC crossover or, equivalently, that these are very strongly coupled superconductors.[4] Finally, the $A_xFe_{2-y}Se_2$ is claimed to be close to an orbital-dependent Mott transition[5] indicating a certain resemblance with the cuprates, although several studies support the microscopic coexistence of superconductivity with magnetism and concomitant insulating states.[6]

Recently, we reported the observation of superconductivity in yet another anisotropic, transition-metal based chalcogenide i.e., $Nb_2Pd_{0.81}S_5$, which displays extremely large upper critical fields.[7] In contrast to the Fe chalcogenides, this compound crystallizes in the lower symmetry space group $C2/m$ which, according to band structure calculations, leads to a complex Fermi surface (FS) composed of both two-dimensional (2D) and quasi-one-dimensional (Q1D) sheets. The Pd stoichiometry is predicted to play a major role since the calculations indicate that it displaces the Fermi-level favoring nesting among the Q1D FS sheets for particular wave vectors, and this would lead to electronic instabilities and possibly to itinerant magnetism.[7] Therefore, the Pd fraction is expected to play a role similar to that of F or Co and K in the "1111" and "122"Fe arsenides, respectively,[8–10] where variations in their stoichiometry are observed to induce superconductivity or increase the superconducting transition temperature in detriment of antiferromagnetism.

Given its composition and electronic anisotropy, one could expect $Nb_2Pd_{0.81}S_5$ to display physical similarities with transition-metal dichalcogenides such as $2H$-NbS_2 or $1T$-TaS_2, or some of the transition metal trichalcogenides such as $NbSe_3$. The former two compounds display a charge-density wave (CDW) transition followed by superconductivity at lower temperatures,[11,12] while the latter displays two transitions towards CDW phases upon cooling.[13] However, we did not detect any sharp anomaly that could indicate a transition akin to a Peierls instability in $Nb_2Pd_{0.81}S_5$; hence we have no evidence for the coexistence of superconductivity with a density-wave-like state which is claimed to enhance the superconducting upper-critical fields (H_{c2}) in the aforementioned compounds.[14] Furthermore, and despite the similar values of T_c, $Nb_2Pd_{0.81}S_5$ displays remarkably larger H_{c2}s (by a factor of 2 or more depending on orientation) when compared to either NbS_2[15] or $NbSe_2$[16] and, in contrast to both compounds, it also displays a clear concave down curvature in $H_{c2}(T)$ for $H\|b$ axis. These observations indicate few similarities between $Nb_2Pd_{0.81}S_5$ and the dichalcogenide or trichalcogenide compounds. In addition, as we will see below, the properties of the metallic state of compounds emerging from $Nb_2Pd_{0.81}S_5$ by replacing S with Se are non-Fermi liquid like in the region of temperatures just above T_c in contrast to the aforementioned compounds. This behavior is very prominent in a very narrow range of values for the fraction x of Pd, or when $0.67 \leqslant x \leqslant 0.71$, where one observes the emergence of superconductivity from the nonsuperconducting compounds.

In this paper, we show that different families of compounds can be created by varying the chemistry of $Nb_2Pd_{0.81}S_5$, leading to superconducting compounds such as $Nb_2Pd_xSe_5$ and $Nb_3Pd_xSe_7$. It turns out, as shown below, that $Nb_2Pd_xSe_5$ for $x \simeq 0.7$ displays a crossover from metallic ($\partial\rho/\partial T > 0$) to "nonmetallic" ($\partial\rho/\partial T < 0$) upon cooling; therefore, we show that superconductivity in this compound emerges from

an anomalous metallic state. This crossoverlike temperature is observed to decrease as T_c increases (upon variation of x), with the metallic state displaying non-Fermi-liquid behavior as a function of the temperature, i.e., $\rho = \rho_0 + AT^n$ with n ranging from ~1 to ~0.4. In contrast, the $Nb_3Pd_{0.7}Se_7$ compound, with a middle point superconducting transition temperature $T_c \simeq$ 2.1 K, displays Fermi-liquid-like metallic behavior (or $n = 2$) above 150 K. Nevertheless, a mild anomaly centered around 110 K is observed in the resistivity, suggesting also a crossover or perhaps an electronic instability. Although in this compound T_c increases with x or the Pd content, the position of this anomaly remains unaffected by it. Similar to the $Nb_2Pd_xSe_5$ compounds, superconductivity in the $Nb_3Pd_xSe_7$ series also emerges from a state displaying nonmetallic character (or $\partial\rho/\partial T < 0$).

For these chalcogenides, low dimensionality, multiband effects, anomalous metallic behavior, and as will be discussed below for the case of $Nb_3Pd_{0.7}Se_7$, anisotropic and extremely high upper critical fields, suggest an unconventional super-conducting state. Here, we focus on the superconducting phase diagram of $Nb_3Pd_{0.7}Se_7$. A detailed account on the dependence of the superconducting phase diagrams of $Nb_2Pd_xSe_5$ and $Nb_3Pd_xSe_7$ on x or the Pd content will be given elsewhere.

II. EXPERIMENT

$Nb_3Pd_{0.7}Se_7$ was grown via a solid state reaction under an Ar atmosphere: Nb (99.99%), Pd (99.99%), and Se (99.999%) well mixed powders in the ratio of 4:1:10 were heated up to a peak temperature of 850 °C at a rate of 100 °C/h in sealed quartz ampoules, kept for 48 h and subsequently quenched to room temperature. The obtained single crystals formed thin long needles several millimeters in length, but with cross-sectional areas ranging from 1×5 μm^2 up to 20×100 μm^2. The stoichiometric composition was determined by energy dispersive x-ray spectroscopy and single-crystal x-ray structure refinement. Two distinct crystallographic phases were identified as resulting from the growth conditions, namely $Nb_3Pd_xSe_7$ and $Nb_2Pd_xSe_5$, with $0.67 \leqslant x \leqslant 0.701$ showing superconducting transition temperatures T_c ranging from $T_c < 0.3$ K up to ~2.0 and ~1.0 K, respectively. The detailed results of our refinements, including the respective atomic positions for typical single crystals of each phase, are given in the Appendix. A conventional four terminal configuration was used for the resistivity measurements which were performed under magnetic fields either by using a physical parameter measurements system (also for heat capacity measurements) or a superconducting magnet coupled to a dilution refrigerator.

Figures 1(a)–1(d) show the resistivity ρ normalized by its value at room temperature, i.e., $\rho/\rho(T = 300 \text{ K})$ as a function of the temperature (in a logarithmic scale) for five single crystals resulting from the same synthesis process. These crystals were analyzed through single-crystal x-ray diffraction measurements to reveal both their composition and their crystallographic structure. Traces in Figs. 1(a) and 1(b) were obtained from crystals belonging to the $Nb_3Pd_xSe_7$ phase, whose Pd content x was refined as $x = 0.676(2)$ (blue trace), $x = 0.68(1)$ (green trace), and $x = 0.7025(22)$ (gray trace), respectively. The room temperature resistivity of these

crystals was found to oscillate between several tenths of $\mu\Omega$ cm to a few hundreds of $\mu\Omega$ cm. This variability in the actual values of the resistivity can be attributed to the error bars in the determination of their geometrical factors, particularly their thickness which, for example, is approximately 1 μm for the superconducting single crystal shown in Figs. 1(a) and 1(b). As seen in the inset of Fig. 1(a), a broad anomaly is observed in the resistivity around $T = 100$ K, indicating either an electronic phase transition akin to a spin-density wave state seen in the Fe-pnictide superconductors[17] or a crossover towards another electronic regime, such as the pseudogap observed in the cuprates.[18] Notice also that just above the superconducting transition ρ displays an uncharacteristic T dependence for a metal, i.e., with a negative $\partial\rho/\partial T$, indicating the existence of a prominent quasiparticle scattering mechanism. Red lines are fits to the power law $\rho = \rho_0 + AT^n$, which yields exponents n ranging from 3.7 for the nonsuperconducting sample to 2 for the superconducting one, thus suggesting that the superconducting sample displays Fermi-liquid behavior already at high temperatures. The higher exponents for the nonsuperconducting samples result from the pronounced upturn in the resistivity observed around 110 K. The overall behavior seen in Figs. 1(a) and 1(b), i.e., a pronounced change in slope at higher temperatures followed by an uncharacteristic nonmetallic like behavior at lower temperatures, is remarkably similar to what is seen in the underdoped regime of, for example, $La_{2-x}Sr_xCuO_4$,[19] although the resistivity in those compounds follows a linear dependence on temperature at higher temperatures.

Figures 1(c) and 1(d) show $\rho/\rho(T = 300 \text{ K})$ for two $Nb_2Pd_xSe_5$ single crystals, i.e., respectively for $x = 0.7$ and $x = 0.67$ resulting from the same synthesis process. Notice the pronounced but progressive increase in resistivity below ~100 K for the $x = 0.7$ sample, suggesting again a continuous or second-order-like electronic phase transition or perhaps a crossover towards a pseudogaplike regime. Therefore, for *both* compounds $x = 0.7$ defines a threshold concentration separating superconducting from nonsuperconducting samples. Remarkably, while the increase in x beyond 0.7 induces superconductivity in $Nb_3Pd_xSe_7$ it is observed to *suppress* superconductivity in $Nb_2Pd_xSe_5$. This suggests that superconductivity is stabilized by small displacements of the Fermi level, or equivalently that in both compounds the Fermi level is located in close proximity to a van Hove singularity. For the $Nb_2Pd_xSe_5$ compounds, we found that the exponent in the power law describing ρ at high temperatures (150 K $\leqslant T \leqslant 300$ K) evolves from a value close to 1 when $x \sim 0.7$ to $n \sim 0.5$ in the superconducting samples (or when $x \simeq 0.67$) which corresponds to non-Fermi-liquid behavior, and cannot be easily ascribed to scattering by phonons. Furthermore, the superconducting transition for $Nb_2Pd_{0.67}Se_5$ is preceded by an upturn in the resistivity starting at $T = 48$ K. Therefore, for both compounds and for $0.67 \leqslant x \lesssim 0.7$ superconductivity condenses out of an unconventional metallic state.

As discussed below as well as in Ref. 7, the geometry of the FS of these compounds is complex and contains quasi-one-dimensional sheets which are the necessary ingredient for a Peierls-like instability, which could lead to itinerant magnetism. The broad anomaly seen around 110 K in $Nb_3Pd_{0.7}S_7$ single crystals could correspond to evidence for such a transition and therefore in Fig. 2(a) we show the
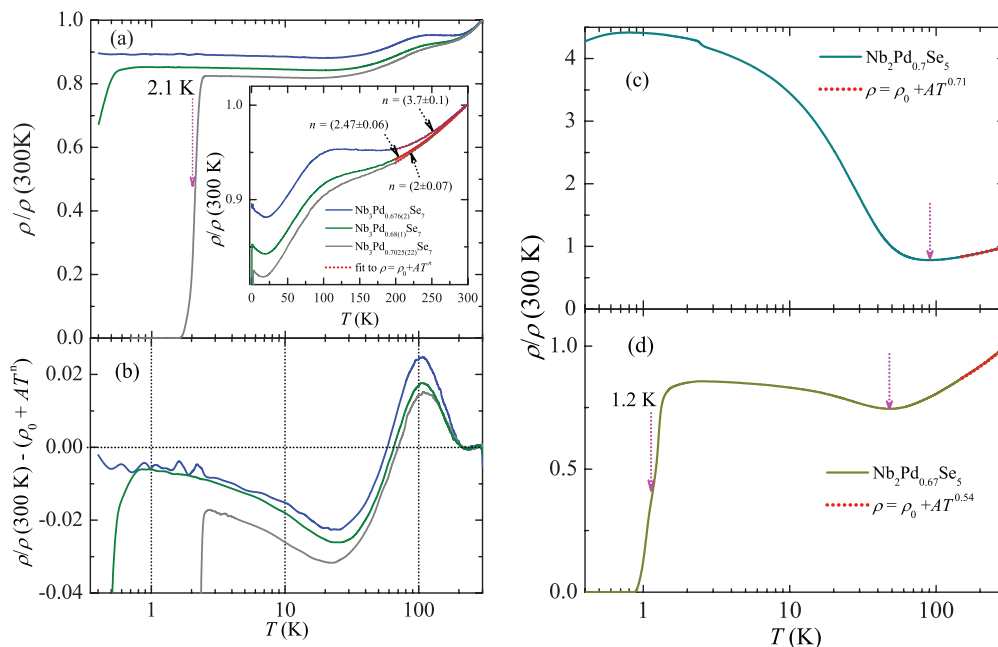
FIG. 1. (Color online) (a) Resistivity ρ normalized by its value at room temperature $\rho(300\,\mathrm{K})$ as a function of the temperature T for three $\mathrm{Nb_3Pd_xSe_7}$ single crystals, i.e., $x = 0.676(2)$ (blue line), 0.68(1) (green line), and $\simeq 0.7$ (gray line), respectively. The dimensions of the superconducting crystal are $\sim 1 \times 10^{-4} \times 8.5 \times 10^{-3} \times 0.2\ \mathrm{cm^{-3}}$, leading to a room temperature resistivity of $\sim 70\ \mu\Omega\,\mathrm{cm}$ (for a contacts separation of $\sim 0.05\ \mathrm{cm}$). Inset: $\rho/\rho(300\,\mathrm{K})$ as a function of T in a linear temperature scale. Red lines are fits to the power law $\rho = \rho_0 + AT^n$ within the range $150 \leqslant T \leqslant 300$ K. The superconducting compound displays Fermi-liquid-like behavior or $n = 2$. (b) $\rho/\rho(300\,\mathrm{K})$ after subtraction of the aforementioned power law. Notice a sharp anomaly at $T^\star \sim 110$ K which is independent on the Pd content x, but whose amplitude is seen to decrease as x increases. This anomaly of unknown origin is followed by a minimum in the resistivity at $T_{\min} \sim 24$ K, suggesting electronic localization preceding the superconducting transition. (c) and (d) Resistivity $\rho/\rho(300\,\mathrm{K})$ as a function of the temperature T for two $\mathrm{Nb_2Pd_xSe_5}$ single crystals, i.e., $x = 0.7$ and 0.67, respectively. Notice the observation of an upturn in the resistivity at a Pd-dependent temperature, indicating again an interplay with some form of electron localization. The characteristic temperature $T_{\min}$ below which ρ becomes nonmetallic decreases as the Pd content decreases. The dimensions of the $\mathrm{Nb_2Pd_{0.67}Se_5}$ single crystal are $\sim 1.75 \times 10^{-4} \times 3.4 \times 10^{-3} \times 0.235\ \mathrm{cm^{-3}}$, leading to a room temperature resistivity of $\sim 225\ \mu\Omega\,\mathrm{cm}$. Red lines are fits to the power-law behavior observed in the metallic state, which yield non-Fermi-liquid-like exponents n ranging from ~ 1 (nonsuperconducting) to ~ 0.4 (in superconducting samples).

magnetic susceptibility χ as a function of the temperature for a batch containing hundreds of randomly oriented single crystals. We used hundreds of crystals, given that a typical individual single crystal, whose data are shown above, weighs only $\sim 1\ \mu$g. We found that this particular batch is composed almost exclusively of crystals belonging to the $\mathrm{Nb_3Pd_xSe_7}$ phase. As seen, at higher temperatures $\chi(T)$ varies little showing an unexpected linear dependence in temperature which could be an indication for Pauli-like susceptibility, but with a temperature-dependent density of states at the Fermi level. Around 110 K one observes just a mild deviation from linearity as indicated by the arrow; hence it does not represent a clear evidence for an electronic or magnetic phase transition. For $T < 50$ K, $\chi(T)$ displays a sharp upturn which, as seen in the inset, does not correspond to a Curie tail: the inset plots the inverse of $\chi(T)$ in a limited temperature, i.e., for $T < 50$ K, and as seen it is not linear in temperature. Consequently, this upturn cannot be attributed to the presence of impurities and most likely corresponds to evidence for magnetic correlations. A fit to a power law yields a very small exponent suggesting a $-\log T$ divergence. Figure 2(b), on the other hand, shows the electronic contribution to the heat capacity C_e normalized by the temperature T, after the

subtraction of a T^3 term and for two values of the field, respectively, $H = 0$ and 9 T. Again, hundreds of single crystals from one synthesis batch (~ 2 mg), therefore of varying stoichiometry, were used for these measurements. A broad anomaly in C_e/T emerges below ~ 1.5 K and peaks at ~ 0.7 K, with its width determined by the distribution of T_c's, as seen in the upper panel. This anomaly is suppressed by the application of an external magnetic field, as expected for bulk superconductivity. Therefore, our observations clearly indicate bulk superconductivity. We emphasize that the data shown in Fig. 1 corresponds to crystals displaying among the highest T_c's within the batches synthesized by us. In contrast, the heat capacity yields an average value for T_c.

$\mathrm{Nb_3Pd_{0.7}Se_7}$ crystallizes in the space group $C2/m$ (see Fig. 3) and can be described as composed of sheets of a single $\mathrm{Nb_6PdSe_{14}}$ basic unit which is comprised of chains formed by square-planar and trigonal-prismatic Se polyhedra which are approximately centered by Pd and Nb atoms, respectively (see Ref. 20). Each chain extends along the [010] direction (needle axis). The Pd(1) atoms center a column of face-to-face square planes. Both Nb(1) and Nb(2) atoms occupy chains of edge-sharing trigonal prisms, while the Nb(3) atoms occupy columns of face sharing trigonal prisms. The
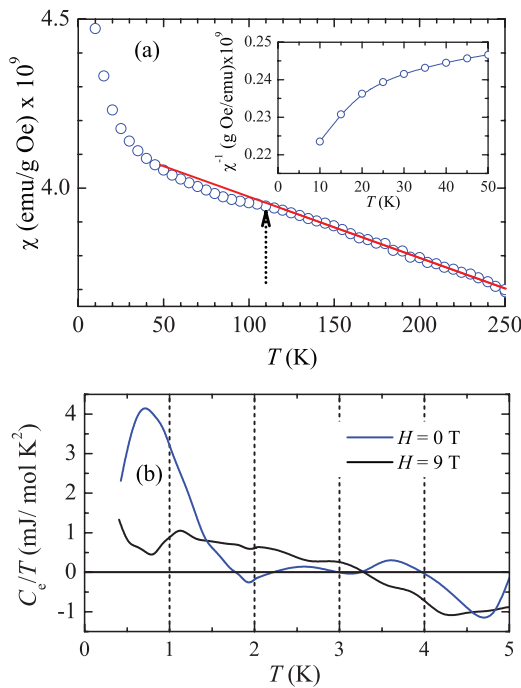
FIG. 2. (Color online) (a) Magnetic susceptibility χ as a function of the temperature for hundreds of single-crystals from a typical synthesis batch. Vertical arrow indicates the deviation from linearity at $T \sim T^\star$ where an anomaly is observed in the resistivity of $Nb_3Pd_xS_7$ single crystals. Inset: χ^{-1} as a function of T at lower temperatures. (b) Heat capacity normalized by T and as a function of T for hundreds of single-crystals from a typical synthesis batch containing both phases. One observes a broad anomaly centered around $T = 0.75$ K, which disappears with the application of a field of 9 T, indicating bulk superconductivity.

basic Nb_6PdSe_{14} is formed in such a way that the polyhedra in adjacent columns share their edges. The Nb_6PdSe_{14} layers form via interdigitation of the Nb_6PdSe_{14} units, with the Nb(3) atoms acquiring a seven-coordinate, monocapped trigonal-

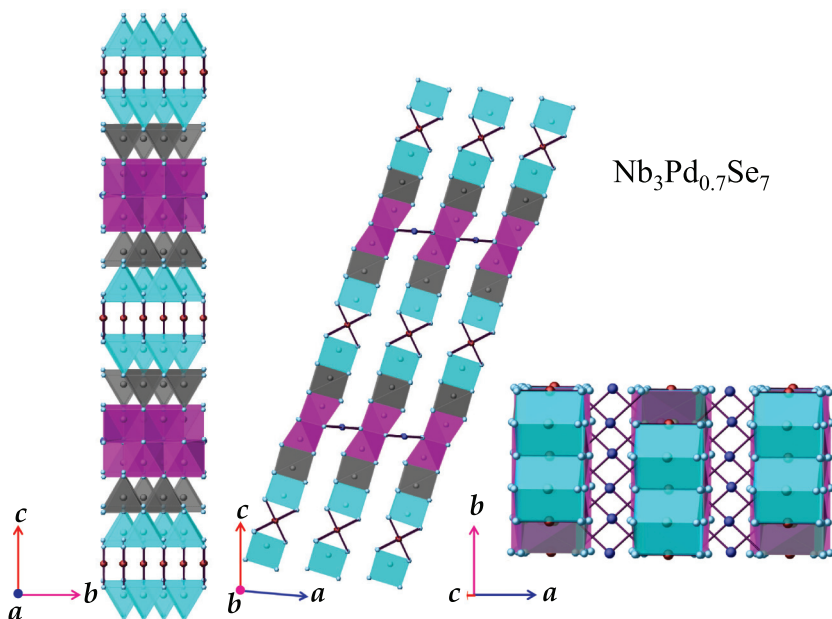FIG. 4. (Color online) (a) Resistivity ρ as a function of the field H applied along the a axis of a $Nb_3Pd_{0.7}Se_7$ single crystal for several temperatures. (b) Same as in (a) but for fields along the c axis and at pumped ^{3}He temperatures. (c) Same as in (a) but for fields along the b axis.

prismatic environment. The three-dimensional structure results from the stacking of these layers in a closed packed (Se atoms) fashion. The Pd(2) atom occupies a rhombic site between the layers and is square-planar coordinated with the Se(1) atoms.

Given the low crystallographic symmetry of $Nb_3Pd_{0.7}Se_7$ one expects an anisotropic response for magnetic fields applied along its distinct crystallographic axis. Therefore, we

$Nb_3Pd_{0.7}Se_7$

FIG. 3. (Color online) (a) From left to right, distinct perspectives of the crystallographic structure of $Nb_3Pd_{0.7}Se_7$: along the a, b, and nearly along the c axis, respectively. The Nb(1), Nb(2), and Nb(3) atoms are depicted in turquoise, gray, and magenta colors, respectively. Pd(1) and Pd(2) atoms are depicted in maroon and dark blue colors, whereas all the Se atoms are depicted in clear blue color, respectively.
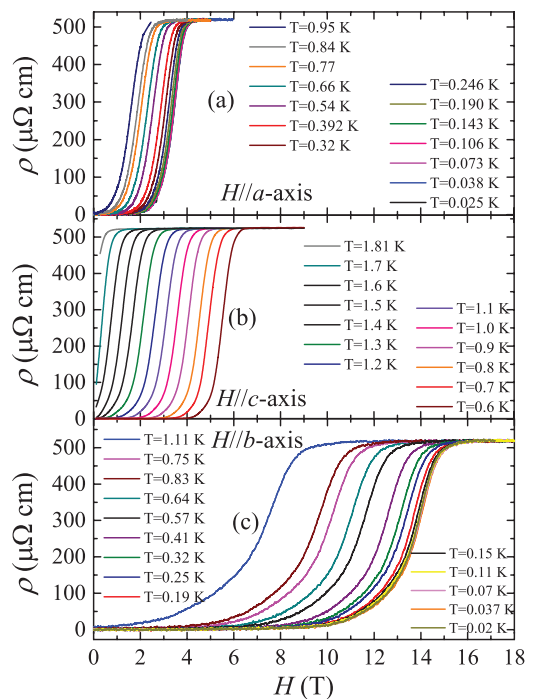
show the resistivity of a second $Nb_3Pd_{0.7}Se_7$ single crystal ($T_c \simeq 1.8$ K) for several temperatures and as a function of the magnetic field H applied along the a and the c axis [Figs. 4(a) and 4(b), respectively] and for fields along the b or the needle axis [Fig. 4(c)]. This crystal was placed onto a sapphire substrate and the external field was initially applied perpendicular to the (b,c) plane [Fig. 4(a)]. Subsequently, the field was rotated by 90° with respect to this previous orientation, while remaining perpendicular to the needle axis [Fig. 4(b)]. Subsequently, it was rotated by 90° around the a axis in order to align the field along the b axis [Fig. 4(c)]. As seen, the resistive transitions from the superconducting to the metallic state for the different field orientations reveal rather anisotropic upper-critical fields H_{c2}.

III. DISCUSSION

In Fig. 5, we display the resulting H_{c2}-T phase diagram, constructed by plotting the middle point of the resistive transitions shown in Fig. 4 as well as from the resistivity as a function of T under field (not shown). Remarkably, H_{c2} for fields along the b axis saturates at a value of $H_{c2}(T \to 0$ K$) \sim 14.1$ T, which is $4.26 \times H_p [= 1.84 T_c$ ($\simeq 1.8$ K)], where H_p is the Pauli limiting field in the weak coupling regime. To put this value in perspective, compare the ratio $H_{c2}(T \to 0$ K$)/T_c = 14.1$ T/1.8 K $= 7.83$ with the
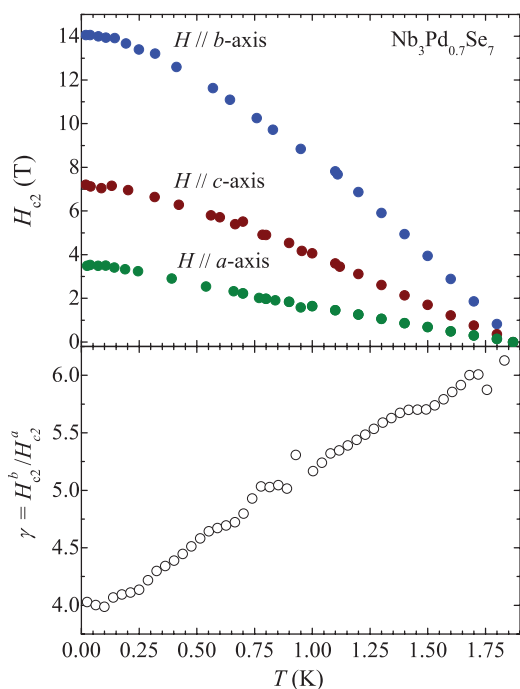

FIG. 5. (Color online) Upper panel: phase boundary between superconducting and metallic states in the temperature (T)–magnetic field (H) plane for $Nb_3Pd_{0.7}Se_7$. Blue markers depict the phase boundary for fields applied along the needle, or the b axis of the crystal. Brown and green markers depict the phase boundary for fields applied along the c axis and the a axis, respectively. Lower panel: anisotropy in upper-critical fields $\gamma = H_{c2}^b/H_{c2}^a$ as a function of temperature. Notice that γ is temperature dependent as previously observed in multiband superconductors.

corresponding ratios for $Fe_{1+y}Se_{0.45}Te_{0.55}$ (~ 50 T/14 K $\simeq$ 3.57)[21], $CeCoIn_5$ (~ 12 T/2.3 K $= 5.2$),[22] and URu_2Si_2 (~ 12.5 T/1.5 K $= 8.33$)[23] which, according to all evidence, are unconventional and strongly correlated superconductors. Notice that this ratio for $Nb_3Pd_{0.7}Se_5$ also surpasses the respective one for $Nb_2Pd_{0.81}S_5$ (~ 37 T/6.6 K $\simeq 5.6$),[7] or for the Chevrel-phase $PbMo_6S_8$ (~ 60 T/13.3 K $\simeq 4.51$),[24] and obviously the ratio for the widely used Nb_3Sn compound (~ 30 T/18 K $\simeq 1.67$).[25] Finally, and although the anisotropy γ for $Nb_3Pd_{0.7}Se_7$ is not as high as the one reported for $Li_{0.9}Mo_6O_{17}$, which suggests that this later compound is considerably more quasi-one-dimensional,[26] its ratio $H_{c2}(T \to 0$ K$)/T_c \sim 15$ T/2.2 K $= 6.82$ still is smaller than the ratio reported here.

Below we show Ginzburg-Landau fittings of the phase boundary, which for fields along the b axis yields an orbital limiting field $H_0 = (35 \pm 3)$ T and $H_p = (19 \pm 1)$ T, therefore suggesting that $Nb_3Pd_{0.7}Se_7$ could be a Pauli limited superconductor displaying a very large Maki parameter $\alpha = \sqrt{2}H_0/H_p = 2.6$ if one uses both field values resulting from the fittings, or $\alpha \simeq 3.5$ if one uses the actual experimental result 14.1 T. In any case, these values for α are > 1.8, the value required for the observation of the Fulde-Ferrel-Larkin-Ovchinikov-state.[27] Below we also show a fit of $H_{c2}^b(T)$ to the Werthamer-Helfand-Hohenberg (WHH) formalism,[28] indicating that a large α value of ~ 2.4 would fit the boundary, but would require a large spin-orbit coupling implying that this coupling is relevant for this system. Finally, as seen in the lower panel of Fig. 5, the superconducting anisotropy $\gamma = H_{c2}^b/H_{c2}^a$ is T dependent as seen in the Fe pnictides/chalcogenides and interpreted as evidence for multiband effects.[29,30]

In order to evaluate the contributions of both orbital and Pauli pair-breaking effects for all field orientations we analyze our $H_{c2}(T)$ data at temperatures close to T_c where the Ginzburg-Landau (GL) theory yields[31]

$$\left(\frac{H}{H_p}\right)^2 + \frac{H}{H_o} = 1 - \frac{T}{T_c}. \tag{1}$$

Very close to the critical temperature, $(T_c - T)/T_c \ll (H_p/H_o)^2$, the first paramagnetic term in the left-hand side is negligible and Eq. (1) yields the orbital linear Ginzburg-Landau temperature dependence, $H_{c2} = H_o(1 - T/T_c)$. At lower temperatures, $(T_c - T)/T_c > (H_p/H_o)^2$, the Pauli limiting field H_p dominates the shape of $H_{c2}(T) \propto (1 - t)^{1/2}$ even in the GL domain if $H_p < H_o$. The latter inequality is equivalent to the condition that the Maki parameter $\alpha \sim H_o/H_p > 1$ is large enough, assuring that the paramagnetic effects are essential. Shown in the upper panel of Fig. 6 are the log-log plots of our $H_{c2}(T)$ as a function of $1 - T/T_c$, where the red lines are fits to Eq. (1). As seen for fields along the b axis (blue markers), the fitting yields $H_p = (19 \pm 0.5)$ T and $H_o = (35 \pm 3)$ T, respectively, implying a Maki parameter of 2.6 if one uses both values resulting from the fittings, or $\alpha \simeq 3.5$ if one used the experimental result 14.1 T as a tentative value for the Pauli limiting field. In any case, such large values for the paramagnetic limiting field relative to T_c would be difficult to understand for a conventional superconductor, suggesting either very strong correlations renormalizing H_p as seen in the heavy fermions, or an unconventional pairing mechanism, or
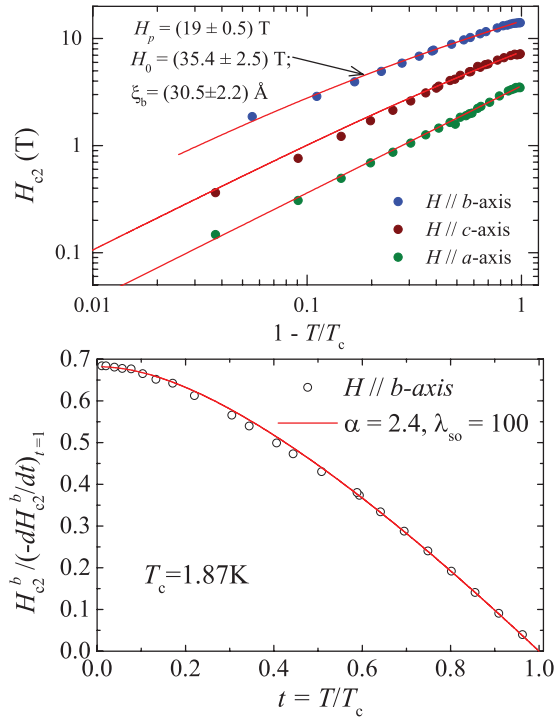
FIG. 6. (Color online) Upper panel: H_{c2} for Nb$_3$Pd$_{0.7}$Se$_7$ as a function of $1 - t$, where $t = T/T_c$, for fields applied along the b axis (blue dots), c axis (brown dots), and a axis (green dots), respectively. Red lines are fits to Eq. (1). Lower panel: H_{c2}^b for fields along the b axis normalized by the linear slope at T_c and as a function of t. Red line is a fit to the WHH formalism.

both. For the other two orientations, one obtains similar values for both H_p and H_o. The lower panel of Fig. 6 shows a fit of H_{c2}^b normalized by the slope of its linear dependence at T_c and as a function of the reduced temperature T/T_c. Red line is a fit to the Werthamer, Helfand, and Hohenberg formalism[28] with a tentative value of the Maki parameter $\alpha = 2.4$, which yields an extremely large value for the spin-orbit coupling parameter $\lambda_{so} = 100$. Although it remains unclear how reliable such a large value is, this suggests that the spin-orbit coupling plays a relevant role for this system.

To shed some light about the possible superconducting pairing mechanism in Nb$_3$Pd$_{0.7}$Se$_5$ we have performed band structure calculations to determine the geometry of the Fermi surface; the results are summarized in Fig. 7. Density functional theory calculations using WIEN2K[32] with the generalized gradient approximation (GGA)[33] to the exchange correlation potential were employed to calculate the self-consistent energy eigenvalues at 16 000 k points in the reciprocal lattice. A doubled cell with one Pd(2) atom removed was used in order to achieve a formula unit of Nb$_6$Pd$_{1.5}$Se$_{14}$, resulting in band folding in the smaller reciprocal space cell. The FSs were calculated using the experimental lattice constants and atomic positions established in this work. The centering symmetry of space group no. 12 ($C2/m$) was eliminated so that half the Pd at the $2a$ Wyckoff position could be removed, resulting in a doubled unit cell with formula Nb$_6$Pd$_{1.5}$Se$_{14}$, i.e., with slightly more Pd than is incorporated experimentally. As seen in Figs. 7(c) and 7(d) the resulting FS is composed of quasi-2D
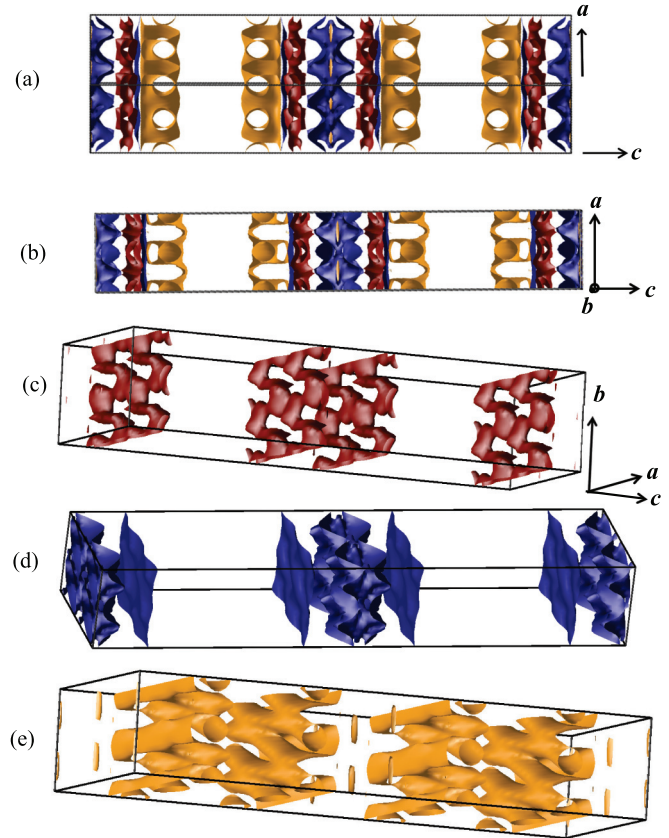

FIG. 7. (Color online) (a) Perspective of the geometry of the Fermi surface of Nb$_3$Pd$_{0.7}$Se$_7$ in a $2 \times 2 \times 2$ conventional reciprocal unit cell as obtained through DFT calculations. (b) Same as in (a) but through a lateral perspective. Maroon and blue FS sheets are holelike, while the gold intersecting cylinders are electronlike in one direction and holelike in the other. Notice that the FS is composed of both quasi-two-dimensional nearly cylindrical sheets as well as highly corrugated quasi-one-dimensional ones. The Q1D surfaces are extremely sensitive to the Fermi energy, which is in turn sensitive to the exact Pd content.

sheets (maroon surfaces) of hole character, and a set of strongly and weakly warped Q1D (blue) sheets of hole character whose geometry is sensitive to the exact Pd content. The complex 3D network itself (golden) seen in Fig. 7(e) contains both hole- and electronlike orbits. Therefore, given that the resulting FS is composed of multiple sheets, having both electron and hole character, this system can indeed be classified as a multiband superconductor. Spin-polarized calculations show that a ferromagnetic state is stable, with a small moment attributable to some Nb atoms [0.27 μ_B/Nb(1) and 0.20 μ_B/Nb(2)] and a polarized, delocalized interstitial density. The stabilization energy is extremely small, and manipulable via variations in the Pd content indicating that the system is in proximity to magnetism. If a spin fluctuation mechanism were in play, T_c might be tunable by varying the stoichiometry as seen here.

IV. SUMMARY

In summary, Nb$_3$Pd$_{0.7}$Se$_7$ is a chalcogenide based multi-band superconductor, displaying extremely large upper critical

fields, i.e., comparable to those of unconventional strongly correlated heavy-fermion superconductors. The synthesis process also yields crystals of the $Nb_2Pd_xSe_5$ phase, which also displays superconductivity. Both compounds display an anomalous metallic behavior, particularly for temperatures above their respective superconducting transitions which bears resemblances with the pseudogap phase of the cuprates. Such anomalous metallic behavior was not observed in $Nb_2Pd_{0.81}S_5$ which displays a considerably higher superconducting transition temperature.[7] This clearly indicates that the fraction x of Pd plays the role of a dopant, i.e., by varying its content one can, for instance, suppress nonmetallic states and stabilize superconductivity as observed in the $Nb_2Pd_xSe_5$ series. Notice that this study was confined to a narrow range in x, from $\sim$0.67 to $\gtrsim$ 0.7, where we have shown that small variations in x or $\Delta x = 0.03$ easily suppress superconductivity in both families of compounds. Therefore, the overall behavior reported here for the $Nb_3Pd_xSe_7$ series is clearly characteristic of an underdoped regime. As we already implied within the Introduction, an anomalous metallic behavior with broad anomalies, which cannot be clearly attributed to phase transitions and which instead suggests crossovers towards other electronic regimes, makes these compounds particularly distinct from the dichalcogenides or the trichalcogenides. Notice that, in quasi-one-dimensional or quasi-two-dimensional systems such as these, both charge-density waves[34] coupling to lattice distortions and spin-density waves[35] resulting from electronic correlations lead to sharp, first-order-like anomalies in their physical properties such as the resistivity,[36] in contrast to what is seen here. In fact, it would seem that these compounds are more akin to the Fe chalcogenide superconductors: for example, in the $Fe_{1+y}Se_xTe_{1-x}$ series the resistivity in the metallic state is known to display a $-\log T$ dependence above

the superconducting transition which can be suppressed upon careful annealing.[21]

A complex Fermi surface composed also of quasi-one-dimensional sheets, interplay of superconductivity with an anomalous metallic state, and extremely high upper critical fields coupled to multiband behavior suggest an unconventional pairing symmetry.

APPENDIX: PARAMETERS OF $Nb_2Pd_{0.67}Se_5$ AND $Nb_3Pd_{0.7}Se_7$ AS DERIVED FROM THE X-RAY REFINEMENTS

Table I contains the crystallographic parameters for two representative superconducting single-crystals, $Nb_2Pd_{0.67}Se_5$ and $Nb_3Pd_{0.7}Se_7$ respectively, as extracted from single-crystal x-ray refinements. Table II on the other hand, contains the resulting positional atomic data for both compounds.

TABLE I. Crystallographic parameters for two superconducting crystals as extracted from single-crystal x-ray refinements.

Compound	$Nb_2Pd_{0.67}Se_5$	$Nb_3Pd_{0.70}Se_7$
Space group	$C2/m$	$C2/m$
a (Å)	12.8325(7)	12.7965(6)
b (Å)	3.39327(18)	3.40591(17)
c (Å)	15.3859(8)	21.0370(13)
β (°)	101.471(5)	95.530(5)
α, γ (°)	90.0	90.0
Z	4	4
V (Å^3)	656.59(6)	912.60(8)
$d_{cal.}$ (g/cm^3)	6.599	6.590
T (K)	298	298
Range (°)	$3.24 < \theta$	$2.92 < \theta$
	<66.41	<45.00
Reflections	6162	4170
Parameters refined	52	70
Goodness of fit	1.0046	1.1150

TABLE II. Positional atomic data for $Nb_2Pd_{0.67}Se_5$ and $Nb_3Pd_{0.70}Se_7$, respectively.

Atom	Site	Occupation	x	y	z	U_{eq}
			$Nb_2Pd_{0.67}Se_5$			
Nb1	4i	1	0.07595(4)	1/2	0.17999(3)	0.0099
Nb2	4i	1	0.15288(4)	0	0.37854(3)	0.0078
Pd1	2a	1	0	0	0	0.0124
Pd2	2c	0.348(5)	0	0	1/2	0.0117
Se1	4i	1	0.35036(5)	0	0.48914(3)	0.0098
Se2	4i	1	0.25374(4)	1/2	0.29566(3)	0.0086
Se3	4i	1	0.17536(5)	0	0.09778(4)	0.0106
Se4	4i	1	0.42303(5)	1/2	0.13214(4)	0.0104
Se5	4i	1	0.50041(4)	0	0.32346(4)	0.0091
			$Nb_3Pd_{0.70}Se_7$			
Atom	Site	Occupation	x	y	z	U_{eq}
Nb1	4i	1	0.05848(5)	1/2	0.12765(3)	0.0105
Nb2	4i	1	0.11676(5)	0	0.26968(3)	0.0083
Nb3	4i	1	0.16833(5)	1/2	0.41178(3)	0.0071
Pd1	2a	1	0	0	0	0.0126
Pd2	2d	0.393(5)	0	1/2	1/2	0.0109
Se1	4i	1	0.35141(6)	1/2	0.49292(3)	0.0089
Se2	4i	1	0.16650(6)	0	0.06770(4)	0.0108
Se3	4i	1	0.40985(6)	1/2	0.09657(4)	0.0103
Se4	4i	1	0.22426(6)	1/2	0.20964(4)	0.0091
Se5	4i	1	0.28063(6)	0	0.35319(3)	0.0078
Se6	4i	1	0.47084(6)	0	0.23370(3)	0.0083
Se7	4i	1	0.02204(6)	0	0.37263(3)	0.0088

*balicas@magnet.fsu.edu

[1] T. M. McQueen, Q. Huang, V. Ksenofontov, C. Felser, Q. Xu, H. Zandbergen, Y. S. Hor, J. Allred, A. J. Williams, D. Qu, J. Checkelsky, N. P. Ong, and R. J. Cava, Phys. Rev. B **79**, 014522 (2009).

[2] M. Burrard-Lucas, D. G. Free, S. J. Sedlmaier, J. D. Wright, S. J. Cassidy, Y. Hara, A. J. Corkett, T. Lancaster, P. J. Baker, S. J. Blundell, and S. J. Clarke, Nat. Mater. **12**, 15 (2013).

[3] A.-m. Zhang, T.-l. Xia, K. Liu, W. Tong, Z.-r. Yang, and Q.-m. Zhang, Sci. Rep. (UK) **3**, 1216 (2013).

[4] Y. Lubashevsky, E. Lahoud, K. Chashka, D. Podolsky, and A. Kanigel, Nature Phys. **8**, 309 (2012).

[5] M. Yi, D. H. Lu, R. Yu, S. C. Riggs, J.-H. Chu, B. Lv, Z. K. Liu, M. Lu, Y.-T. Cui, M. Hashimoto, S.K. Mo, Z. Hussain, C. W. Chu, I. R. Fisher, Q. Si, and Z.-X. Shen, Phys. Rev. Lett. **110**, 067003 (2013).

[6] A. F. May, M. A. McGuire, H. Cao, I. Sergueev, C. Cantoni, B. C. Chakoumakos, D. S. Parker, and B. C. Sales, Phys. Rev. Lett. **109**, 077003 (2012).

[7] Q. Zhang, G. Li, D. Rhodes, A. Kiswandhi, T. Besara, B. Zeng, J. Sun, T. Siegrist, M. D. Johannes, and L. Balicas, Sci. Rep. (UK) **3**, 1446 (2013).

[8] X. H. Chen, T. Wu, G. Wu, R. H. Liu, H. Chen, and D. F. Fang, Nature (London) **453**, 761 (2008).

[9] A. S. Sefat, R. Y. Jin, M. A. McGuire, B. C. Sales, D. J. Singh, and D. Mandrus, Phys. Rev. Lett. **101**, 117004 (2008).

[10] G. F. Chen, Z. Li, G. Li, W. Z. Hu, J. Dong, J. Zhou, Z. D. Zhang, P. Zheng, N. L. Wang, and J. L. Luo, Chin. Phys. Lett. **25**, 3403 (2008).

[11] For recent results, see V. G. Tissen, M. R. Osorio, J. P. Brison, N. M. Nemes, M. García-Hernandez, L. Cario, P. Rodière, S. Vieira, and H. Suderow, Phys. Rev. B **87**, 134502 (2013).

[12] For recent results, see T. Ritschel, J. Trinckauf, G. Garbarino, M. Hanfland, M. v. Zimmermann, H. Berger, B. Büchner, and J. Geck, Phys. Rev. B **87**, 125135 (2013).

[13] See, for example, A. A. Sinchenko and P. Monceau, Phys. Rev. B **87**, 045105 (2013) and references therein.

[14] A. M. Gabovich, A. I. Voitenko, and M. Ausloos, Phys. Rep. **367**, 583 (2002).

[15] B. W. Pfalzgraf and H. Spreckels, J. Phys. C: Solid State Phys. **20**, 4359 (1987).

[16] D. Sanchez, A. Junod, J. Muller, H. Berger, and F. Levy, Physica B **204**, 167 (1995); N. Toyota, H. Nakatsuji, K. Noto, A. Hoshi, N. Kobayashi, Y. Muto, and Y. Onodera, J. Low Temp. Phys. **25**, 485 (1976).

[17] See, for example, R. H. Liu, G. Wu, T. Wu, D. F. Fang, H. Chen, S. Y. Li, K. Liu, Y. L. Xie, X. F. Wang, R. L. Yang, L. Ding, C. He, D. L. Feng, and X. H. Chen, Phys. Rev. Lett. **101**, 087001 (2008).

[18] T. Timusk and B. Statt, Rep. Prog. Phys. **62**, 61 (1999).

[19] H. Takagi, B. Batlogg, H. L. Kao, J. Kwo, R. J. Cava, J. J. Krajewski, and W. F. Peck, Jr., Phys. Rev. Lett. **69**, 2975 (1992).

[20]D. A. Keszler and J. A. Ibers, J. Am. Chem. Soc. **107**, 8119 (1985).

[21]T. Gebre, G. Li, J. B. Whalen, B. S. Conner, H. D. Zhou, G. Grissonnanche, M. K. Kostov, A. Gurevich, T. Siegrist, and L. Balicas, Phys. Rev. B **84**, 174517 (2011).

[22]A. Bianchi, R. Movshovich, C. Capan, P. G. Pagliuso, and J. L. Sarrao, Phys. Rev. Lett. **91**, 187004 (2003).

[23]J. P. Brison *et al.*, Physica C **250**, 128 (1995); Physica B **199**, 70 (1994).

[24]K. Okuda, M. Kitagawa, T. Sakakibara, and M. Date, J. Phys. Soc. Jpn. **48**, 2157 (1980).

[25]B. T. Matthias, T. H. Geballe, S. Geller, and E. Corenzwit, Phys. Rev. **95**, 1435 (1954); R. M. Scanlan, A. P. Malozemoff, and D. C. Larbalestier, Proc. IEEE **92**, 1639 (2004).

[26]J.-F. Mercure, A. F. Bangura, X. Xu, N. Wakeham, A. Carrington, P. Walmsley, M. Greenblatt, and N. E. Hussey, Phys. Rev. Lett. **108**, 187003 (2012).

[27]L. W. Gruenberg and L. Gunther, Phys. Rev. Lett. **16**, 996 (1966).

[28]N. R. Werthamer, E. Helfand, and P. C. Hohenberg, Phys. Rev. **147**, 295 (1966).

[29]H. Q. Yuan, J. Singleton, F. F. Balakirev, S. A. Baily, G. F. Chen, J. L. Luo, and N. L. Wang, Nature (London) **457**, 565 (2009).

[30]A. Yamamoto, J. Jaroszynski, C. Tarantini, L. Balicas, J. Jiang, A. Gurevich, D. C. Larbalestier, R. Jin, A. S. Sefat, M. A. McGuire, B. C. Sales, D. K. Christen, and D. Mandrus, Appl. Phys. Lett. **94**, 062511 (2009).

[31]A. Gurevich, Phys. Rev. B **82**, 184504 (2010).

[32]P. Blaha, K. Schwarz, P. Sorantin, and S. B. Trickey, Comput. Phys. Commun. **59**, 399 (1990); K. Schwarz and P. Blaha, Comput. Mater. Sci. **28**, 259 (2003).

[33]J. P. Perdew, K. Burke, and M. Ernzerhof, Phys. Rev. Lett. **77**, 3865 (1996).

[34]G. Grüner, Rev. Mod. Phys. **60**, 1129 (1988).

[35]G. Grüner, Rev. Mod. Phys. **66**, 1 (1994).

[36]See, for example, N. Biškup, S. Tomić, and D. Jérome, Phys. Rev. B **51**, 17972 (1995).